# Measurement of Ultrasound-Enhanced Diffusion Coefficient of Nanoparticles in an Agarose Hydrogel

Dong Ma[1], Jeffrey S. Marshall[2] and Junru Wu[1]

[1]Department of Physics
[2]Department of Mechanical Engineering
The University of Vermont
Burlington, Vermont, U.S.A.

Corresponding Author: Junru Wu, Department of Physics, The University of Vermont, Burlington, VT 05405, U.S.A. PHONE: 1 (802) 656-8357, EMAIL: jwu@uvm.edu.

Keywords: biofilms, oscillating diffusion, nanoparticles, ultrasound

Running title: Acoustic enhancement of diffusion in a hydrogel

## Abstract

An experimental study has been performed to measure the effect of ultrasound on nanoparticle diffusion in an agarose hydrogel. Agarose hydrogel is often used as a simulant for biofilms and certain biological tissues, such as muscle and brain tissue. The work was motivated by recent experiments indicating that ultrasonic excitation of moderate intensity can significantly enhance nanoparticle diffusion in a hydrogel. The objective of the current study was to obtain detailed measurements of the effect of ultrasound on nanoparticle diffusion in comparison to the molecular diffusion in the absence of acoustic excitation. Experiments were conducted with 1 MHz ultrasound waves and nanoparticle diameters of 20nm and 100nm, using fluorescent imaging to measure particle concentration distribution. Under ultrasound exposure, the experiments yield estimates for both acoustic diffusion coefficients as well as acoustic streaming velocity within the hydrogel. Measured values of acoustic streaming velocity were on the order of 0.1 μm/s, which agree well with a theoretical estimate. Measured values of the acoustic diffusion coefficient were found to be 74% larger than the molecular diffusion coefficient of the nanoparticles for 20nm particles and 133% larger than the molecular diffusion coefficient for 100nm particles.

## 1. Introduction

A biofilm consists of bacteria immersed in a network of proteins called extracellular polymeric substances (EPS), through which nutrients and minerals necessary for growth of the bacteria are transported. Diffusion is the primary mechanism for transport of particles and chemicals in a biofilm (Stewart, 2003; Zhang et al., 2011). A promising method for delivery of antibiotics to bacterial colonies within biofilms is via attachment to liposomes, nanoparticles or lipid-polymer hybrid nanoparticles, with particle sizes below 100nm being found optimal for use as a carrier (Forier et al., 2014a, 2014b; Li et al., 2015; Cheow et al., 2011). One mechanism by which biofilms protect bacteria is by chemically deactivating antimicrobial agents in the outer EPS layers of the biofilm. Encapsulation of these antimicrobial agents within liposomes or solid nanoparticles can be effective for carrying the antibiotic past this chemical barrier. Liposomes and nanoparticles can also be targeted to attach to bacterial outer membranes, thereby delivering the antibiotic agent directly to the bacterial cell (Forier et al., 2014a).

It was observed by Ma et al. (2015) that low intensity ultrasound (far below the intensity necessary to induce acoustic cavitation) can significantly enhance transport of liposomes into an alginate gel, including both the liposome transport from solution to the hydrogel outer surface and liposome penetration into the gel. Similar acoustic enhancement of diffusive processes in more general porous media was noted by Vogler and Chrysikopoulos (2002) for the problem of diffusion of a passive tracer in a packed column of glass spheres. These authors proposed a phenomenological model that accounted for the acoustic enhancement effect by introducing a modified diffusion coefficient that is a function of the amplitude of particle velocity of the acoustic wave in situ.

A stochastic model was proposed by Marshall (2016) for acoustic diffusion coefficient of particles in a porous medium. The model assumes that the diffusion of a particulate phase in a porous medium is produced by the combination of acoustic oscillations and random retention, where the latter is produced by hindered motion of the diffused phase by the pore walls of the porous medium. Retention occurs in a variety of diffusion processes when the diffusing material is partially or temporarily blocked by structures within the conducting medium (Bevilacqua et al., 2011). In the case of polymeric gels, such as biofilms or hydrogels, retention is associated with the phenomenon of *hindered diffusion*, in which the transport rate of solute molecules and nanoparticles is reduced by near-wall effects as the large molecules or particles pass through small pores within the gel (Buck et al., 1999; Kätelhön and Compton, 2014). A study of the effects of hindered diffusion on nanoparticle diffusion within agarose gels was given by Fatin-Rouge et al. (2004).

While previous work suggests that ultrasound excitation can enhance the diffusion of nanoparticles within a hydrogel, there are no detailed measurements to verify this hypothesis or to characterize the exact extent of diffusion enhancement by ultrasound excitation. The objective of the current study is to conduct detailed experiments that measure diffusion in a hydrogel of different size particles both without ultrasound (called the *control* samples) and with ultrasound exposure (called the *treated* samples). The experiments verify the effect of ultrasound on enhancement of nanoparticle diffusion within a hydrogel and provide a measurement of the enhanced diffusion coefficient. In order to make the porous medium more uniform between experimental runs, we performed our experiments with an agarose hydrogel instead of a natural biofilm. Alginate and agarose hydrogels are common physical models for biofilms since they share similar extracellular matrix, porous structures and mechanical properties (Jung et al., 2015;

Rowley et al., 1990; Smidsrød et al., 1990), but the agarose or alginate hydrogels have the advantages of fast setup and consistent properties and thickness compared to natural biofilms. Use of agarose hydrogel in this study allows our experiments to be more consistent and controlled than would be the case with living biofilms.

The experimental method is described in Section 2. The method for analysis of experimental data to extract diffusion coefficients is described in Section 3. The experimental results and related discussion are presented in Section 4. Conclusions are given in Section 5.

## 2. Experimental Method

The agarose hydrogel was formed using a 0.8% agarose solution, which was prepared by adding 0.8g agarose to a 98ml, 50mM calcium chloride solution in a 125ml flask. The solution was mixed using a magnetic stirring bar, placed in a microwave oven for 1 minute's heating, and then moved back to a magnetic stirrer and mixed at a temperature of $90\,°C$ . Meanwhile, 2ml of 5% sodium dodecyl sulfate (SDS) (5g per 100ml) was added to the solution. A sample of 40ml of the agarose solution was moved to another flask, to which was added 2ml of fluorescent sphere suspension (FluoSpheres, F8803, ThermoFisher, USA). The solution was then continuously mixed at the same temperature. At this point, the experimental procedure resulted in one flask of clear agarose solution and another flask of fluorescent agarose solution. The experiments were performed using a two-layer agarose model, which was formed by first moving 12ml of the clear agarose solution to a petri dish and letting it sit for 3 minutes to form the first gel layer. The second layer was formed by seeding 10ml of the agarose mixture with fluorescent spheres, and then pouring it on top of the first layer and letting it sit for another 3 minutes until a gel formed.

The ultrasound transducer used in experiments was a single-element non-focusing piezo-ceramic transducer (Olympus NDT Inc., Waltham, MA) operated at 1.0 MHz, with active radius $b$ = 9.5 mm and Rayleigh distance $a_R = b^2 / \lambda \cong 6.0\,\text{cm}$. The transducer was immersed in water and suspended a distance of about 1cm over the hydrogel sample, so the hydrogel was clearly in the transducer near-field region and the acoustic waves can be taken to be approximately one-dimensional (Lewin and Ziskin, 1992). An arbitrary waveform function generator (33250A, Agilent, Santa Clara, CA) was programmed to produce a tone-burst sinusoidal signal with 20% duty cycle for insonation duration $t_A$ of either 5 or 10 minutes, and the output of the waveform generator was used as the input of a 55 dB RF power amplifier (ENI A300, Rochester, NY) whose output was used to drive the transducer. The spatially- and temporally-averaged intensity ($I_{SATA}$) used in the experiment was 2.32 W/cm$^2$, which was measured by using the radiation force measurement (Beissner, 1993). A schematic diagram showing the experimental setup is given in Figure 1. In each case where the hydrogel was exposed to ultrasonic excitation (which we call the *treated sample*), another sample from the same gel was extracted that was not exposed to ultrasound (called the *control sample*).

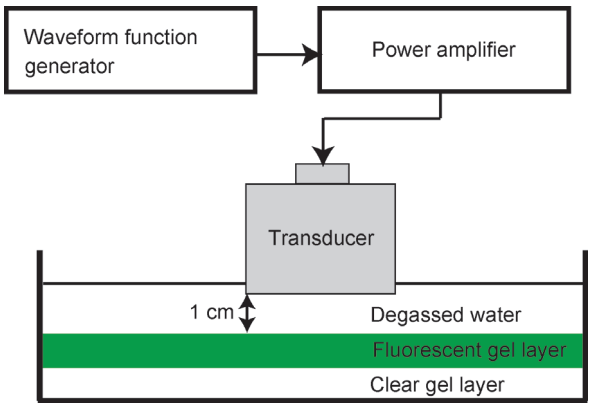


Figure 1. Experimental set-up for measuring ultrasound-enhanced diffusion of nanoparticles. (Not to scale)

Optical imaging of the hydrogel to measure fluorescent intensity profile was performed after a time interval $t_f$ following gel formation. A sample of the hydrogel was obtained by cutting a cross section out of the two-layer agarose layer for each run. Imaging of the sample was performed using a computer-controlled confocal microscope (Zeiss LSM 510 META) to obtain the fluorescence intensity profile. An example of this process is shown in Figure 2. A sample of the fluorescent hydrogel is shown in Fig. 2a. At the initial time, the sample appears green on its left side (which is initially seeded with fluorescent particles) and it is clear on its right side (with no initial particles). Over time, the fluorescent particles diffuse from the particle-rich left-hand side to the particle-poor right-hand side, producing a more gradual fluorescence intensity distribution as shown in Fig. 2a. The corresponding fluorescence intensity profile was obtained by averaging the measurements from three repeated experiments. An example fluorescence intensity profile is shown in Fig. 2b, which plots fluorescence intensity versus distance along the imaging plane (denoted by $x$). The origin of the distance coordinate $x$ is set as the location where the imaging plane intersects the boundary between the two hydrogel layers.

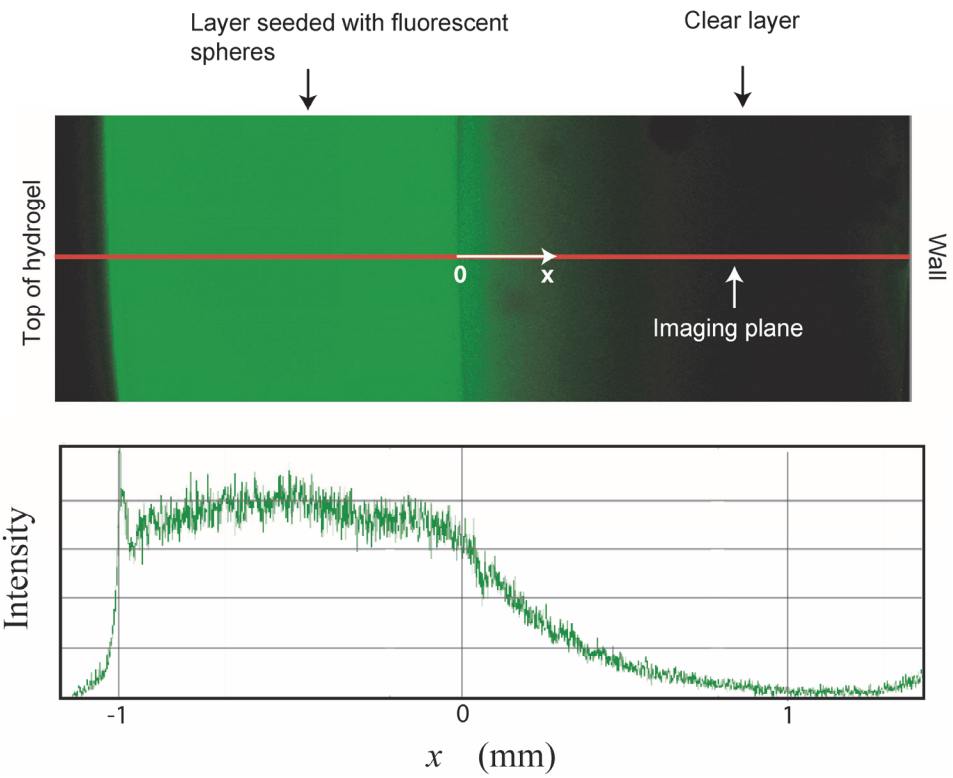


Figure 2. Plots showing an example of the fluorescent imaging of the hydrogel. (a) Image of fluorescent gel showing two layers and imaging plane. The left-hand layer is initially seeded with fluorescent particles and the right-hand layer is initially clear. (b) Example showing fluorescence intensity variation with distance $x$ on the imaging plane.

## 3. Data Analysis

The fluorescence data was processed to estimate the diffusion coefficient by numerical solution for the particle concentration $c(x,t)$ for both the treated samples (samples with ultrasound exposure) and for the control samples (samples without ultrasound exposure). It is assumed that the molecular diffusion coefficient $D_M$ (associated with thermal molecular motion) and the acoustic diffusion coefficient $D_A$ (associated with enhancement of diffusion via ultrasonic excitation) are additive, so that the total diffusion coefficient can be written as

153

154 $$D = D_M + D_A . \tag{1}$$

155

156 For the treated samples, we wish to estimate both the acoustic streaming velocity and the
157 acoustic contribution $D_A$ to the diffusion coefficient. For control samples, we wish to estimate
158 the molecular diffusion coefficient $D_M$. For convenience, the concentration is normalized by its
159 initial value $c_0$ within the part of the film that is seeded with fluorescent particles. The particle
160 concentration is proportional to the fluorescence intensity $J(x,t)$, such that

161

162 $$\hat{c}(x,t) \equiv \frac{c(x,t)}{c_0} = \frac{J(x,t)}{J_0}, \tag{2}$$

163

164 where $\hat{c}(x,t)$ is the normalized concentration and $J_0$ is the initial fluorescence intensity of the
165 seeded part of the film.

166 The normalized concentration for the control samples is governed by the standard
167 diffusion equation

168

169 $$\frac{\partial \hat{c}}{\partial t} = D_M \frac{\partial^2 \hat{c}}{\partial x^2} \qquad \text{for } 0 \le t \le t_f, \tag{3}$$

170

171 where *t* is time since formation of the hydrogel, *x* is depth within the agarose hydrogel film, and
172 $t_f$ is the time period that imaging is performed following hydrogel formation. The initial particle
173 concentration is assumed to be a step function $\hat{c}(x,0) = 1 - U(x)$, where the step function is

defined by $U(x) = 0$ for $x < 0$ and $U(x) = 1$ for $x \geq 0$. The origin $x = 0$ coincides with the discontinuity in the initial fluorescence distribution (the position in-between the two layers of the hydrogel). The final value of $\hat{c}(x,t)$ at time $t_f$ for the control samples is denoted by $F_C(x) \equiv \hat{c}(x, t = t_f)$.

For the samples that have been treated with ultrasound, it is convenient to split the molecular and acoustic diffusion processes into two parts. The molecular diffusion process is the same as for the control samples, whereas the additional acoustic diffusion process involves both a diffusion term associated with the acoustic diffusion coefficient $D_A$ and an acoustic streaming term associated with the (constant) streaming velocity *u*. Letting $\tau$ be a pseudo time variable, the additional nanoparticle transport caused by the combination of advection by acoustic streaming and acoustic diffusion is governed by the advection-diffusion equation

$$\frac{\partial \hat{c}}{\partial \tau} + u\frac{\partial \hat{c}}{\partial x} = D_A \frac{\partial^2 \hat{c}}{\partial x^2} \qquad \text{for } 0 \leq \tau \leq t_A, \tag{4}$$

where $t_A$ is the time interval over which ultrasound excitation is applied. Equation (4) is solved numerically with the initial condition $\hat{c}(x, \tau = 0) = F_C(x)$, and the final value of the normalized concentration obtained from (4) at $\tau = t_A$ is denoted by $F_T(x) \equiv \hat{c}(x, \tau = t_A)$.

We note that the acoustic radiation pressure may also potentially influence particle motion. However, the radiation force is proportional to the particle volume (King, 1934) whereas the Stokes drag is proportional to particle diameter *d*. The ratio of the radiation force to the Stokes drag is proportional to $d^2$, indicating that the radiation force becomes negligible for sufficiently small particle diameters. An analysis (and experimental validation) of the effect of

196 acoustic radiation force versus acoustic streaming on suspended particles was given by Barnkob
197 et al. (2012), who found that the particle acoustic streaming velocity $u_{str}$ was approximately
198 equal to the velocity $u_{rad}$ induced by acoustic radiation force for particles of diameter
199 $d_{crit} \cong 1.4\,\mu\text{m}$ in water. The largest particles used in the current experiments have diameter of
200 100 nm, for which case we would expect the ratio $u_{rad} / u_{str} \cong 0.005$. While the above estimate
201 was made for particles in water, it should be reasonably valid for nanoparticles that are
202 sufficiently small to move in the aqueous solution within the pore space of the agarose hydrogel.
203 As a final confirmation that radiation force is negligible in our experiments, we note that our
204 measured results for particle velocity *u* are nearly independent of particle size, which does not fit
205 the hypothesis that acoustic radiation pressure plays a significant role in the particle motion. By
206 contrast, the acoustic streaming velocity is independent of particle diameter, so the hypothesis
207 that particles are advected with the acoustic streaming velocity is in good agreement with our
208 findings.

209 It is convenient to define dimensionless variables $x' = x/L$ and $t' = t/T$, where the
210 length scale $L$ is set equal to the measurement depth in the film and the time scale $T$ is set equal
211 to $t_f$ in the molecular diffusion problem (3) and to the ultrasound exposure time $t_A$ for the
212 acoustic diffusion problem (4). The diffusion problem is solved on the interval $-2 \le x' \le 1$ with
213 a Dirichlet boundary condition $\hat{c}(-2,t') = 1$ on the left-hand side and the Neumann boundary
214 condition $\partial\hat{c} / \partial x'(1,t') = 0$ on the right-hand side. The resulting dimensionless problem for
215 molecular diffusion on the control samples is given by

216

217 $$\frac{\partial \hat{c}}{\partial t'} = D'_M \frac{\partial^2 \hat{c}}{\partial x'^2} \qquad \text{for } 0 \le t' \le 1 \text{ and } -2 \le x' \le 1 \qquad (5)$$

with initial condition $\hat{c}(x',0) = 1 - U(x')$. The dimensionless problem for acoustic diffusion on the treated samples is given by

$$\frac{\partial \hat{c}}{\partial t'} + u' \frac{\partial \hat{c}}{\partial x'} = D'_A \frac{\partial^2 \hat{c}}{\partial x'^2} \qquad \text{for } 0 \le t' \le 1 \text{ and } -2 \le x' \le 1. \tag{6}$$

The dimensionless acoustic streaming velocity $u'$ and diffusion coefficient $D'$ are defined by

$$u' = uT / L, \qquad D' = DT / L^2. \tag{7}$$

Numerical solution of (5) and (6) was performed using the Crank-Nicholson method for the diffusion terms and second-order upwind differencing for the advection term. Computations are performed with time and spatial steps sizes $\Delta t' = 0.001$ and $\Delta x' = 0.01$.

The experimental data for the control and treated normalized concentration fields measured at imaging time $t_f$ are denoted by $\hat{e}_C(x)$ and $\hat{e}_T(x)$, respectively. For the control samples, a least-square error measure $E_C$ was defined by the integral over the domain $0 \le x' \le 1$ of the square of the difference between the experimental data for the control samples and the result $F_C(x') \equiv \hat{c}(x',1)$ of the numerical solution of (5), giving

$$E_C \equiv \int_0^1 [\hat{e}_C(x') - F_C(x')]^2 \, dx', \tag{8}$$

The numerical computation of (5) was repeated for a range of values of $D'_M$ and the error $E_C$ for each case was tabulated. The optimal value of $D'_M$ was selected as that which yields a minimal value of $E_C$.

For the treated samples, a similar least-square error measure was defined by

$$E_T \equiv \int_0^1 [\hat{e}_T(x') - F_T(x')]^2 \, dx', \tag{9}$$

where $F_T(x') \equiv \hat{c}(x',1)$ is the numerical solution of (6). The numerical computation of (6) was repeated for a range of values of both $u'$ and $D'_A$, and the error $E_T$ for each case was tabulated. Optimal values of $u'$ and $D'_A$ were selected as those which yielded a minimal value of $E_T$.

## 4. Results and Discussion

A summary of the parameter values for the different experimental runs conducted is given in Table 1. Experiments for particle diffusion were performed with particles of diameter 20nm and 100nm. No diffusion was observed in experiments conducted with even larger particles, with 200nm diameter, from which we deduce that the pore size of the hydrogel must be between 100-200nm. In Table 1, the length scale *L* indicates the depth that imaging is performed into the hydrogel below the interface ( $x = 0$ ) separating the layer initially seeded with fluorescent particles from the unseeded layer. Each experiment is denoted as either molecular (for control samples with no ultrasound exposure) or acoustic (for treated samples with ultrasound exposure). For molecular experiments, the time scale *T* denotes the time period $t_f$ at which imaging is performed following initial formation of the hydrogel. For the acoustic

261 experiments, the time scale $T$ denotes the length of the time interval $t_A$ that the hydrogel is
262 exposed to ultrasound.
263
264 Table 1. List of experimental cases examined and relevant parameters.

| Case | Particle diameter (nm) | Length scale $L$ (μm) | Exposure time $T$ (min) | Acoustic or Molecular |
|---|---|---|---|---|
| Set 1.1 | 20 | 763.805 | 15 | Molecular |
| Set 1.2 | 20 | 763.805 | 30 | Molecular |
| Set 1.3 | 20 | 763.805 | 45 | Molecular |
| Set 2.1 | 20 | 393.75 | 15 | Molecular |
| Set 2.2 | 20 | 393.75 | 5 | Acoustic |
| Set 3.1 | 100 | 393.75 | 70 | Molecular |
| Set 3.2 | 100 | 393.75 | 10 | Acoustic |

265
266 A set of experiments (Set 1.1-1.3) was first conducted with 20 nm diameter particles to
267 examine time variation of the molecular diffusion results, in order to confirm that the observed
268 phenomenon is adequately described by the diffusion equation. Imaging results for particle
269 fluorescence were taken at intervals of 15 min, 30 min and 45 min following hydrogel formation.
270 The experimental results for concentration profile are compared in Figure 3 with predictions
271 from numerical solution of (5) starting with a step function initial condition, indicated by lines at
272 the three different times. For this experiment, the best-fit molecular diffusion coefficient is given
273 by $D_M = 54.0\ \mu m^2/s$, which is used for all three prediction curves in Figure 3 and is observed to
274 provide a good fit to the experimental data.

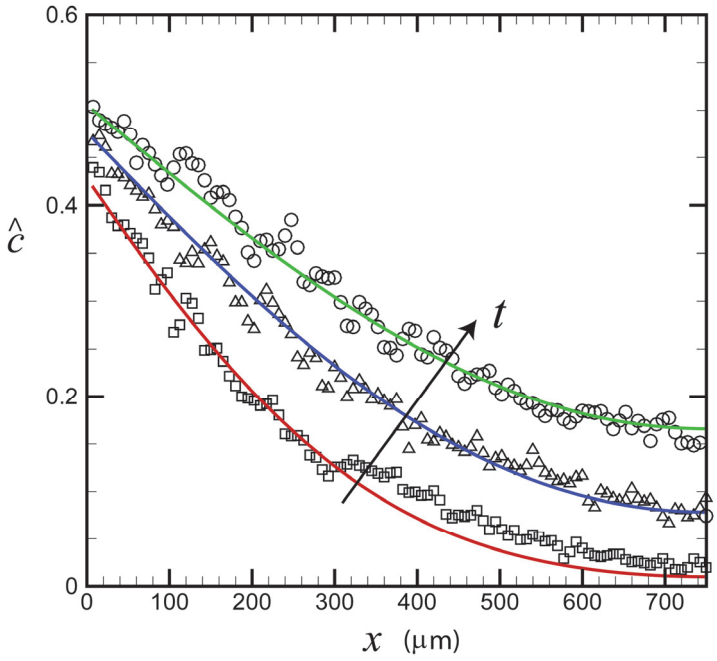


Figure 3. Comparison of experimental data and prediction from solution of the diffusion equation for 20 nm diameter particles with molecular diffusion (no ultrasound) at three different imaging times. Experimental data are shown at times $t_f$ after hydrogel formation of 15 minutes (square symbols), 30 minutes (delta symbols), and 45 minutes (circular symbols). Predictions are shown for a best-fit molecular diffusion coefficient of $D_M = 54$ μm$^2$/s, starting from a step function initial condition, at times 15 min (red line), 30 min (blue line) and 45 min (green line). (Color online)

For the experiments with acoustically-enhanced diffusion, three different sets of experiments were performed using three different hydrogels on different days for each case examined. One case was also repeated a total of 10 times in order to verify that the uncertainty does not change significantly with increase in sample size. The first set of experiments (Set 2.1-2.2) was performed for 20nm diameter particles, and the second set of experiments (Set 3.1-3.2) was performed for 100nm diameter particles. Best-fit values for the diffusion coefficient and

290 (when applicable) for the acoustic streaming velocity from these experiments are recorded in
291 Table 2, including both dimensionless and dimensional values.
292
293 Table 2. List of best-fit diffusion coefficient and acoustic streaming velocity for the different
294 experimental cases. Both dimensionless values (primed) and dimensional values are listed.

| Case | Streaming Velocity, $u'$ (dimensionless) | Molecular Diffusion Coefficient, $D'_M$ (dimensionless) | Acoustic Diffusion Coefficient, $D'_A$ (dimensionless) | Streaming Velocity, $u$ (μm/s) | Molecular Diffusion Coefficient, $D_M$ (μm$^2$/s) | Acoustic Diffusion Coefficient, $D_A$ (μm$^2$/s) |
|---|---|---|---|---|---|---|
| Set 1.1 | - | 0.0865 | - | - | 54.0 | - |
| Set 1.2 | - | 0.173 | - | - | 54.0 | - |
| Set 1.3 | - | 0.258 | - | - | 54.0 | - |
| Set 2.1 | - | 0.232 | - | - | 40.0 | - |
| Set 2.2 | 0.12 | - | 0.134 | 0.157 | - | 69.4 |
| Set 3.1 | - | 0.103 | - | - | 3.80 | - |
| Set 3.2 | 0.20 | - | 0.0342 | 0.131 | - | 8.84 |

295

296 Results for the experiments with 20nm diameter particles are shown in Figure 4. The
297 control data are denoted using deltas and the ultrasound treated data using circles. The numerical
298 prediction of (5) for molecular diffusion in the control data is indicated by a red line, and the
299 best-fit numerical solution of (6) for the treated data is indicated by a blue line. Both curves fit
300 the experimental data very well. The acoustic diffusion coefficient $D_A$ for the 20 nm particles
301 was found to be 1.74 times the molecular diffusion coefficient $D_M$. The value of molecular
302 diffusion coefficient for Set 2.1 is about 25% lower than the molecular diffusion coefficient

obtained from the results in Set 1.1-1.3, which is likely attributable to variation in the hydrogel structure from one experiment to another.

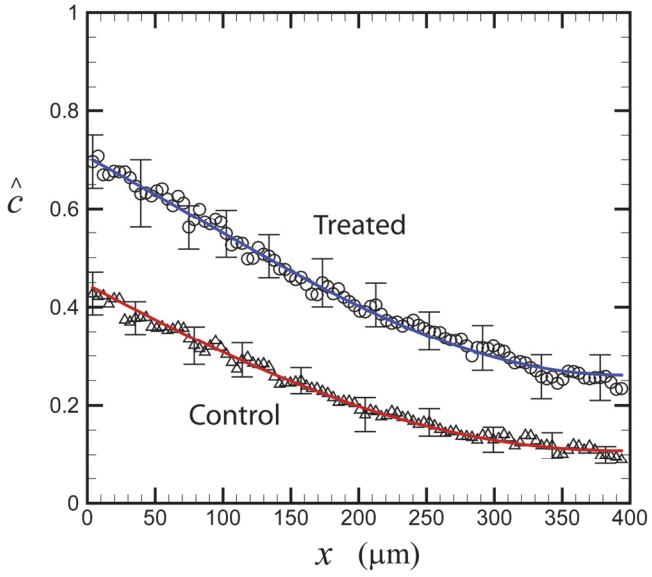


Figure 4. Comparison of data and prediction for 20 nm particles. Data is shown for the control group (deltas) and the treated group (circles) after 10 minutes ultrasound exposure. The measurement was made 70 minutes after the experiment onset. The lower solid line (red color online) indicates the prediction for a molecular diffusion coefficient $D_M = 40.0$ μm$^2$/s, starting from a step function initial condition. The upper solid line (blue color online) represents the prediction for an acoustic diffusion coefficient $D_A = 69.4$ μm$^2$/s and an acoustic streaming velocity of $u = 0.157$ μm/s, with the control group data as an initial condition. Error bars represent root-mean-square of experimental data.

A plot showing the control data (deltas, Set 3.1) and the treated data (circles, Set 3.2) for the experiments with 100nm diameter particles is given in Figure 5. The best prediction from numerical solution of (5) for the molecular diffusion is indicated by the red line. The best prediction from numerical solution of (6) for acoustic-enhanced diffusion is indicated by the blue

line in Figure 5, which was obtained using the experimental data for the control sample as an initial value. The measured acoustic diffusion coefficient for 100nm diameter particles is 2.3 times larger than the molecular diffusion coefficient for the given ultrasound conditions used for this experiment. It is noted that the diffusion coefficients for the 20nm particles are nearly an order of magnitude larger than those for the 100nm diameter particles, whereas the best-fit acoustic streaming velocity differs only by about 20% between the two sets of particles. This difference in acoustic streaming velocity could easily be accounted for by experimental uncertainty or differences in the hydrogel samples that were tested for the two experimental sets.

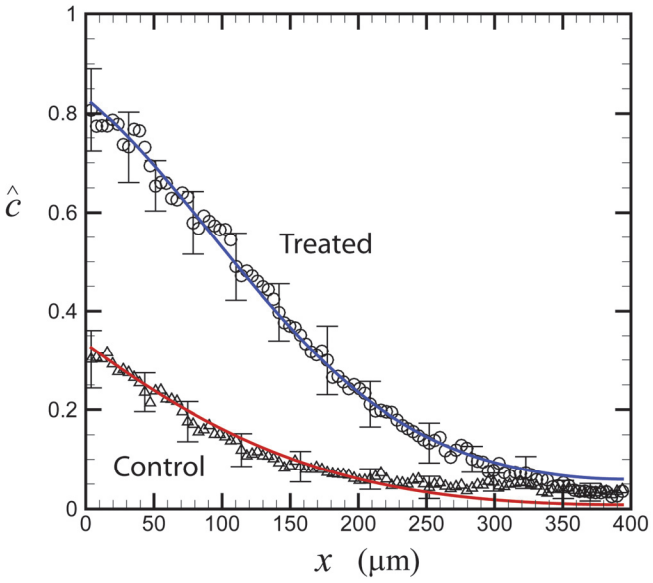


Figure 5. Comparison of data and prediction for 100 nm particles. Data is shown for the control group (deltas) and the treated group (circles) after 10 minutes ultrasound exposure. The measurement was made 70 minutes after the experiment onset. The lower solid line (red color online) indicates the prediction for a molecular diffusion coefficient $D_M = 3.80$ μm$^2$/s, starting from a step function initial condition. The upper solid line (blue color online) represents the prediction for an acoustic diffusion coefficient $D_A = 8.84$ μm$^2$/s and an acoustic streaming

335 velocity of $u = 0.131$ μm/s, with the control group data as an initial condition. Error bars
336 represent root-mean-square of experimental data.
337
338
339 The measured values of acoustic streaming velocity of the particles can be compared to
340 the theoretical expression

341 $$U_0 = \frac{\alpha_F \delta_V^2 I_{SATA}}{\mu c}. \qquad (10)$$

342 obtained by Green et al. (2016) via a scaling estimate. Here, $\alpha_F$ is the acoustic attenuation
343 coefficient, $\delta_V$ is a characteristic length scale for viscous dissipation of the fluid flow, $\mathbf{I}_{SATA}$ is
344 the spatial-average and temporal-average acoustic intensity, $\mu$ is the fluid viscosity, and $c$ is the
345 speed of sound. The attenuation coefficient for agarose hydrogels varies with agar dosage and
346 ultrasound frequency. A study using an agarose gel similar to that examined in the current study,
347 and at the same ultrasound frequency $f = 1$ MHz, was reported by Menikou and Damianou
348 (2017) for a hydrogel used as a muscle simulant. This study gave the acoustic attenuation
349 coefficient and speed of sound in the hydrogel as $\alpha_F \cong 0.05$ Np/m and $c = 1529$ m/s. This
350 attenuation coefficient is about 2.5 times that of pure water. The viscosity of hydrogels also
351 varies widely, with cited values ranging from 0.1-1000 Pa·s; however, a typical value is $\mu \cong 10$
352 Pa·s (Paquet-Mercier et al., 2016). The viscous dissipation length scale $\delta_V$ is assumed to be on
353 the order of the hydrogel film thickness, about $\delta_V \cong 1$mm. Substituting these values into (10)
354 gives an estimate for the order of magnitude of the acoustic streaming velocity as
355 $U_0 = \mathrm{O}(0.1\mu\mathrm{m})$, which is consistent with the measured values shown in Table 2.

The stochastic model of Marshall (2016) assumes that the nanoparticles move via a series of discrete time steps $\Delta t$ with an oscillation velocity amplitude $A$. At each time step, there is a probability $\alpha$ that retention will occur and the particle will not move during that time step. Marshall (2016) showed that in the limit of many time steps, the stochastic process reduces to the solution of a diffusion equation, where the effective acoustic diffusion coefficient $D_A$ is related to the parameters of the stochastic model by

$$D_A = \frac{\alpha}{4} A^2 \Delta t \ . \tag{11}$$

The time step $\Delta t$ in (11) represents the time interval at which retention decisions occur within the porous medium. Setting $\Delta t$ equal to the time interval required for the particle to move a distance of one pore size $a$ of the porous matrix gives $\Delta t = O(a/A)$. Substituting this estimate into (11) yields the acoustic diffusion coefficient as $D_A = O(\alpha A a)$. The particle velocity amplitude $A$ in a pure fluid is related to the acoustic intensity amplitude $I_0$ by $A = \left(2I_0/\rho c\right)^{1/2}$. A pore size for the current study is estimated as $a \cong 200$ nm, based on our observation that 200nm diameter particles did not diffusion in the hydrogel. Using the above estimate for $A$ gives $A \cong 0.17$ m/s for our experiments, which results in $D_A = O(\alpha \times 10^4 \, \mu\text{m}^2/\text{s})$. A retention probability $\alpha$ of about 0.1-1% gives values for acoustic diffusion coefficient in the range of the observed values. It is likely that the particle velocity amplitude $A$ would be lower in a porous medium due to the effect of the pore walls on impeding particle motion. As noted in the review by Wham et al. (1996) for the problem of a spherical particle in a tube, the presence of the

377 confining walls of the tube can increase drag on the particle by up to 1-2 orders of magnitude
378 depending on the ratio of the particle radius to the tube radius.
379
380 **5. Conclusions**
381 An experimental study was conducted to measure the effect of ultrasound excitation on
382 diffusion of nanoparticles in a hydrogel. The experiments were conducted with 20nm and 100nm
383 particles in an agarose hydrogel film of about 1mm thick, using a 1 MHz ultrasound source.
384 Measurements of the molecular diffusion coefficient were obtained with no acoustic excitation,
385 and then measurements were conducted using the same hydrogel of acoustic streaming velocity
386 and acoustic diffusion coefficient in the presence of ultrasound excitation. The diffusion
387 coefficients and streaming velocity were estimated by selecting a best fit between experimental
388 measurements of the film fluorescence intensity profile and numerical predictions from solution
389 of the advection-diffusion equation. The order of magnitude of the measured values of the
390 streaming velocity and acoustic diffusion coefficient were found to compare reasonably well
391 with theoretical estimates using parameter values typical of the agarose hydrogel.
392 The current detailed experimental study confirms the hypothesis proposed by Ma et al.
393 (2015) that ultrasonic excitation can significantly enhance nanoparticle diffusion in a hydrogel.
394 The mechanism for this enhancement proposed by Marshall (2016) is also in reasonable
395 agreement with our measured results. This finding has potential significance for injecting
396 material into biofilms, such as injection of lipid shells containing antibiotics for biofilm
397 mitigation or injection of nutrients to promote biofilm growth. The observation that ultrasound
398 emission enhances nanoparticle diffusion is also relevant to issues involving nanoparticle
399 transport in tissues, for which ultrasound excitation of drug-encapsulated liposomes and

nanoparticles are sometimes used for targeted drug delivery (Tiukinhoy-Laing et al., 2006; Paul et al., 2014; Schroeder et al., 2009; Huang, 2008; Wu et al., 2006).

## Acknowledgements

The authors wish to thank Matthew Wargo for useful discussions on this research. This work was supported by NASA under cooperative agreement number NNX16AQ96A.

409 **References**


410 Barnkob, R., Augustsson, P., Laurell, T., and Bruus, H., Acoustic radiation- and streaming-
411 induced microparticle velocities determined by microparticle image velocimetry in an ultrasound
412 symmetry plane. *Physical Review E* **86**, 056307 (2012).

413

414 Bevilacqua, A.C., Galeão, N.R., and Costa, F.P., A new analytical formulation of retention
415 effects on particle diffusion processes. *Anais da Brasileira de Ciências* (*Annals of the Brazilian*
416 *Academy of Sciences*) **83**(4), 1443-1464 (2011).

417

418 Beissner, K., Radiation force and force balances. In *Ultrasonic Exposimetry*, Lewin, P.A. &
419 Ziskin, M.C. (Eds.), CRC Press Inc., Boca Raton, pp. 127-142 (1993).

420

421 Buck, K.K.S., Dungan, S.R., and Phillips, R.J., The effect of solute concentration on hindered
422 gradient diffusion in polymeric gels. *Journal of Fluid Mechanics* **396**, 287-317 (1999).

423

424 Cheow, W.S., Chang, M.W., and Hadinoto, K., The roles of lipid in anti-biofilm efficacy of
425 lipid-polymer hybrid nanoparticles encapsulating antibiotics. *Colloids and Surfaces A:*
426 *Physicochemical and Engineering Aspects* **389**, 158-165 (2011).

427

428 Fatin-Rouge, N., Starchev, K., and Buffle, J., Size effects on diffusion processes within agarose
429 gels. *Biophysical Journal* **86**, 2710–2719 (2004).


430

Forier, K., Messiaen, A.S., Raemdonck, K., De Smedt, S., Demeester, J., Coenye, T., and Braeckmans, K., Probing the size limit for nanomedicine penetration into *Burkholderia multivorans* and *Pseudomonas aeruginosa* biofilms. *Journal of Controlled Release* **195**, 21-28 (2014a).

Forier, K., Raemdonck, K., De Smedt, S.C., Demeester, J., ye, T., and Braeckmans, K., Lipid and polymer nanoparticles for drug delivery to bacterial biofilms. *Journal of Controlled Release* **190**, 607-623 (2014b).

Green, A.M., Marshall, J.S., Ma, D., and Wu, J.R., Acoustic streaming and thermal instability of flow generated by ultrasound in a cylindrical container. *Physics of Fluids* **28**, 104105 (2016).

Huang, S.L., Liposomes in ultrasonic drug and gene delivery. *Advanced Drug Delivery Reviews* **60**, 1167-1176 (2008).

Jung, Y.-G., Choi, J., Kim, S.-K., Lee, J.-H., and Kwon, S., Embedded biofilms, a new biofilm model based on the embedded growth of bacteria. *Applied and Environmental Microbiology* **81**(1), 211-219 (2015).

Kätelhön, E., and Compton, R.G., Understanding nano-impacts: impact times and near-wall hindered diffusion. *Chemical Science* **5**, 4592-4598 (2014).

King, L.V., On the acoustic radiation pressure of spheres. *Proceedings of the Royal Society of London A* **147**(861), 212-240 (1934).

Lewin, P.A., and Ziskin, M.C., An overview of ultrasonic exposimetry and its clinical relevance. In *Ultrasonic Exposimetry,* M.C. Ziskin and P.A. Lewin (eds.), CRC Press, p. 50 (1992).

Li, X., Yeh, Y.C., Giri, K., Mout, R., Landis, R.F., Prakash, Y.S., and Rotello, V.M., Control of nanoparticle penetration into biofilms through surface design. *Chemical Communications* **51**, 282-285 (2015).

Ma, D., Green, A.M., Willsey, G.G., Marshall, J.S., Wargo, M.J., and Wu, J.R., Effects of acoustic streaming from moderate-intensity pulsed ultrasound for enhancing biofilm mitigation effectiveness of drug-loaded liposomes. *Journal of the Acoustical Society of America* **138**(2), 1043-1051 (2015).

Marshall, J.S., A model of ultrasound-enhanced diffusion in a biofilm. *Journal of the Acoustical Society of America* **139**(6), EL228-EL233 (2016).

Menikou, G., and Damianou, C., Acoustic and thermal characterization of agar based phantoms used for evaluating focused ultrasound exposures. *Journal of Therapeutic Ultrasound* **5**, 14 (2017). DOI 10.1186/s40349-017-0093-z

475 Moudjed, B., Botton, V., Henry, D., Ben Hadid, H., and Garandet, J.-P., Scaling and dimensional
476 analysis of acoustic streaming jets. *Physics of Fluids* **26**, 093602 (2014).
477
478 Nyborg, W.L., Acoustic streaming. In *Physical Acoustics*, Mason, W.P. Ed., IIB. Academic
479 Press, New York, pp. 265-331 (1965).
480
481 Paquet-Mercier, F., Gashti, P., Bellavance, M.J., Taghavi, S.M., and Greener, J., Through thick
482 and thin: a microfluidic approach for continuous measurements of biofilm viscosity and the
483 effect of ionic strength. *Lab on a Chip* **16**(24), 4710-4717 (2016).
484
485 Paul, S., Nahire, R., Mallik, S., and Sarkar, K., Encapsulated microbubbles and achogenic
486 liposomes for contrast ultrasound imaging and targeted drug delivery. *Computational Mechanics*
487 **53**, 413-436 (2014).
488
489 Rowley JA, Madlambayan G, Mooney DJ . Agarose hydrogels as synthetic extracellular matrix
490 materials. *Biomaterials* **20**(1), 45-53 (1999).
491
492 Schroeder, A., Kost, J., and Barenholz, Y., Ultrasound, liposomes, and drug delivery: principles
493 for using ultrasound to control the release of drugs from liposomes. *Chemistry and Physics of*
494 *Lipids* **162**, 1-16 (2009).
495
496 Smidsrød, O., and Skjåk-Brik, G., Agarose as immobilization matrix for cells. *Trends in*
497 *Biotechnology* **8**, 71-78 (1990).

Stewart, P.S., Diffusion in biofioms. *Journal of Bacteriology* **185**(5), 1485–1491 (2003).

Tiukinhoy-Laing, S.D., Huang, S., Klegerman, M., Holland, C.K., McPherson, D.D., Ultrasound-facilitated thrombolysis using tissue-plasminogen activator-loaded echogenic liposomes. *Thrombosis Research* **119**(7), 777-784 (2006).

Vogler, T., and Chrysikopoulos, C.V., Experimental investigation of acoustically enhanced solute transport in porous media. *Geophysical Research Letters* **29**(15), 1710 (2002).

Wham, R.M., Basaran, O.A., and Byers, C.H., Wall effects on flow past solid spheres at finite Reynolds number. *Industrial & Engineering Chemistry Research* **35**(3), 864-874 (1996).

Wu, J., Chen, D., Pepe, J., Himberg, B., and Mercedes, R., Application of liposomes to sonoporation. *Ultrasound in Medicine and Biology* **32**(3), 429–437 (2006).

Wu, J. and Du, G., Temperature elevation in tissues generated by finite-amplitude bursts of ultrasound. *Journal of the Acoustical Society of America* **88**(3), 1562-1577 (1990).

Zhang, Z., Nadezhina, E., and Wilkinson, K.J., Diffusion in a biofilm of *Streptococcus mutans*. *Antimicrobial Agents and Chemotherapy* **55**(3), 1075–1081 (2011).

522

## Figure Captions

Figure 1. Experimental set-up for measuring ultrasound-enhanced diffusion of nanoparticles.

Figure 2. Plots showing an example of the fluorescent imaging of the hydrogel. (a) Image of fluorescent gel showing two layers and imaging plane. (b) Example showing fluorescence intensity variation with distance on the imaging plane. (Color online)

Figure 3. Comparison of data and prediction for 20 nm particles with molecular diffusion (no ultrasound) at three different imaging times: 15 minutes (squares), 30 minutes (deltas), and 45 minutes (circles). Predictions are shown for a best-fit molecular diffusion coefficient of $D_M = 54$ μm$^2$/s, starting from a step function initial condition, at times 15 min (red line), 30 min (blue line) and 45 min (green line). (Color online)

Figure 4. Comparison of data and prediction for 20 nm particles. Data is shown for the control group (deltas) and the treated group (circles) after 10 minutes ultrasound exposure. The measurement was made 70 minutes after the experiment onset. The lower solid line (red color online) indicates the prediction for a molecular diffusion coefficient $D_M = 40.0$ μm$^2$/s, starting from a step function initial condition. The upper solid line (blue color online) represents the prediction for an acoustic diffusion coefficient $D_A = 69.4$ μm$^2$/s and an acoustic streaming velocity of $u = 0.157$ μm/s, with the control group data as an initial condition. Error bars represent root-mean-square of experimental data.

Figure 5. Comparison of data and prediction for 100 nm particles. Data is shown for the control group (deltas) and the treated group (circles) after 10 minutes ultrasound exposure. The measurement was made 70 minutes after the experiment onset. The lower solid line (red color online) indicates the prediction for a molecular diffusion coefficient $D_M = 3.80$ μm$^2$/s, starting from a step function initial condition. The upper solid line (blue color online) represents the prediction for an acoustic diffusion coefficient $D_A = 8.84$ μm$^2$/s and an acoustic streaming velocity of $u = 0.131$ μm/s, with the control group data as an initial condition. Error bars represent root-mean-square of experimental data.